Crack-free Nanosecond Laser Processing of Mechanically Enhanced Tungsten-rhenium Alloys

Haotian Yang*[1], Ryo Yasuhara[1,2], Hiroyuki Noto[1,2], Chihiro Suzuki[1,2], Reina Miyagawa[3], and Hiyori Uehara*[1,2]

[1] *The Graduate University for Advanced Studies, SOKENDAI, 322-6 Oroshi-cho, Toki, Gifu, Japan*
[2] *National Institute for Fusion Science, 322-6 Oroshi-cho, Toki, Gifu, Japan*
[3] *Nagoya Institute of Technology, Gokiso-cho, Showa-ku, Nagoya, Aichi, Japan*
Corresponding author's e-mail: yang.haotian@nifs.ac.jp, uehara.hiyori@nifs.ac.jp

Laser processing of tungsten-rhenium alloys was investigated using a nanosecond Q-switched Nd:YAG laser system. The laser processing properties of a tungsten-rhenium alloy was evaluated in detail. The dependence of the processing hole size and processing depth on different laser fluences was characterized and the development of machined holes produced in different tungsten-rhenium alloys was analyzed. Furthermore, the ablation properties of pure tungsten and tungsten-rhenium alloys were investigated. The high-doped tungsten-rhenium alloy is experimentally confirmed to have better inhibitory effect on cracks and lowest ablation threshold. This results indicate the tungsten-rhenium alloys are expected to be the next-generation nuclear fusion reactor material.
DOI: 10.2961/jlmn.2022.03.2005
Keywords: laser ablation, tungsten-rhenium alloy, surface modification

1. Introduction

Tungsten (W) has many excellent physical characteristics, such as a high melting point, low sputtering yield, hardness, excellent corrosion resistance, and good electrical and thermal conductivity. W has currently become one of the most important functional materials in modern industry and high-tech applications. [1]. It should be noted that the application of W in the field of nuclear fusion is also relevant due to its excellent properties, and W is the most promising candidate for plasma-facing material in fusion reactors [2-6]. Much research is currently focused on customized microstructure changes, surface property modification and texture of W based alloys [7]. These surface treatments help improve performance by reducing friction, wear and plane stress, as well as improving chip flow and extending tool life. Various effects could lead to the generation of cracks on the surface of the material during the surface treatment. Among them, hot tearing (solidification cracking) is one of the most common causes of cracks. In contrast, crack-free surface treated material is even more attractive due to its excellent mechanical properties, such as toughness, ductility and strength [8,9]. Laser processing is generally considered to be an effective and repeatable manufacturing technique that can be used for surface engineering applications in hard and super-hard materials [10,11]. Therefore laser processing of W has been a hot topic, and the study of laser ablation is even more important for the characterization of material properties. The efficiency of material removal from a surface under irradiation with a high-intensity laser is known as the laser ablation rate, which gives the maximum material ablation thickness during laser irradiation [12,13]. The laser ablation properties of W when using a femtosecond ultrafast laser with a pulse width of 100 fs at the central wavelength of 800 nm, were reported in 2010; a single-shot threshold fluence of approximately 0.44 J/cm^2 was obtained for W [14]. In 2017, a Q-switched Nd:YAG laser system with a 5 ns pulse duration and a 20 Hz repetition rate at the central wavelength of 532 nm was used to investigate the laser incubation coefficients of W in air and water, which were determined to be 0.75 and 0.67, respectively [15].

W metal is also frequently used to make alloys and super-alloys that have extremely high melting points and resistance to thermal creep, which enables strengthening of the alloys. Laser processing of W alloys has also attracted widespread attention. Laser processing of WC-Co cemented carbides using Nd:YAG and Nd:YVO_4 nanosecond lasers, and a Ti:sapphire femtosecond laser was reported in 2005, where it was demonstrated that coated/uncoated WC-Co parts can be laser-machined to increase the functionality of their surfaces [16]. Furthermore, an investigation on the effect of the partial dissolution of W carbide on the microstructural evolution by laser clad processing was reported, by which a method to improve surface properties with a Nd:YAG laser system was revealed [17]. The influence of the W doping concentration of a diamond-like nanocomposite film on the ablation and graphitization behavior of the films was very recently investigated using a nanosecond KrF laser system with a wavelength of 248 nm and a picosecond Yb:YAG laser system with a wavelength of 1030 nm [18]. Much research on tungsten alloys has supported the benefits of alloying W with rhenium (Re) to improve the mechanical properties of conventionally fabricated parts. Such alloys not only retain the high melting point and high sputtering threshold of pure tungsten, but also have features such as higher re-crystallization temperatures, increased mechanical strength, increased ductility, and suppressed irradiation hardening [19-24]. We consider that W-Re alloy could be a promising candidate material for new generation of nuclear fusion reactors. However, there is still no relevant research on the laser processing of W-Re alloys. There are also only a few reports on the ablation

rate characterization of nanosecond Nd:YAG laser processing of pure W.

In this study, we investigated the processing properties of W and W-Re alloys using a nanosecond Q-switched Nd:YAG laser system with second harmonic generation as the processing light source. We demonstrate the development of machined craters produced in different materials and present the dependence of the laser-machined hole size and processing depth on the laser fluence, which characterizes the ablation properties of pure W and W-Re alloys. To the best of our knowledge, this is the first study on the laser processing of W-Re alloys. The experimental results presented herein indicate that W-Re alloys are expected to become a new generation of materials in the field of nuclear fusion science.

2. Experiment

Figure 1 shows the experimental setup of the laser processing system employed in this work and laser beam profile at focal position. A Q-switched nanosecond Nd:YAG laser (SAGA PRO 220-20 SHG, Thales Laser S.A) was employed as the processing light source. The processing central wavelength was 532 nm and the pulse width was 8 ns with a repetition frequency of 2 Hz. The applied laser processing energy was from 0.02–2 mJ. The diameter of the laser spot after a plano-convex spherical lens with a focal length of 200 mm was approximately 50 μm.

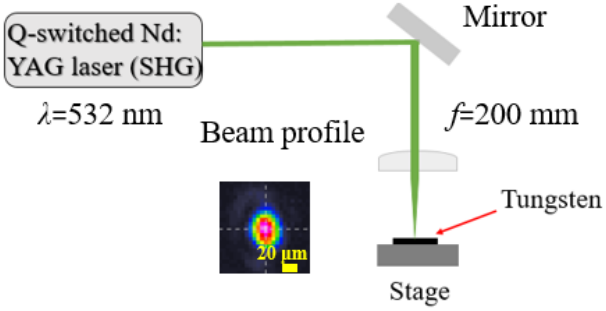

Fig. 1 Schematic diagram of the laser processing system.

ITER grade pure W (A.L.M.T. Corp.) and W-Re (A.L.M.T. Corp.) alloys with different Re doping concentrations (1%, 5%, 25%) were employed as processing samples. The typical grain diameter of the sample is 1 μm. In addition, the samples were polished using P2400 (PRESI) abrasive paper. After polishing, the material had a reflectance from 15–20% at a wavelength of 532 nm and a surface roughness (*R*a) of 0.8–1.2 μm. The physical properties of pure W, W-Re alloy and Re are shown in Table 1. These data indicate that W-Re alloy has higher density and tensile strength. Better mechanical properties can effectively solve the problem of fracture of metal joints in plasma facing components. Therefore, W-Re alloys have significant potential as next-generation nuclear fusion reactor materials. Field emission scanning electron microscopy (FE-SEM; JEOL, JSM-7100F) and laser microscopy (Keyence, VK-X1000) were employed for observation of the machined surface and measurement of the machined surface shape, respectively.

Table 1 Physical properties of W, W-Re alloy and Re

Material	W	W-Re 25% [25]	Re
Melting point (°C)	3422	3021 3400(1%)[26]	3186
Moh's hardness	7.5	--	7.0
Density (g.cm^{-3})	19.3	19.7	21.0
Thermal conductivity (W·m^{-1}·K^{-1})	173	--	48
Thermal expansion coefficient (K)	4.5x10^{-6}	4.9x10^{-9}	6.2x10^{-6}
Work function (eV)	4.5	--	5.0
Tensile strength (kg/mm^2)	200	240	--

3. Results and discussion

Figure 2 shows FE-SEM images of processing craters generated by 100 pulses on (a) pure W (b) W-1% Re (c) W-5% Re, and (d) W-25% Re at a laser fluence of 100 J/cm^2. The distribution of tungsten and rhenium elements was uniform in all our samples according to an analysis of the EDX mapping. The machined hole of the sample has a relatively clear round shape. There is accumulation due to thermal processes [27] around each laser-machined crater, which is one of the characteristics of nanosecond laser processing; that evaporated by heat is cooled, accumulated and re-solidified. The typical processing stack height of the laser-machined crater was approximately 20 μm. A continuous uninterrupted fracture from one point to another with a length of longer than 1 μm within an area range of 10 μm x 10 μm is called one “crack”. At higher resolution, in the deepest area of the machined hole, the numbers of visible cracks were 40–60 (pure W), 10–30 (1% Re), and 10–20 (5% Re), while the 25% Re sample was crack-free. Each sample was processed at more than a dozen craters to count cracks, and the number of cracks was the average of each sample. The cracks in the laser-machined holes were significantly reduced as the doping concentration of Re increased, which is due to the effect of Re to increase the dislocation mobility and increase ductility by the promotion of better plastic flow [28]. Therefore, the highly doped W-Re alloy has better crack suppression ability. For all samples at high resolution, some balling phenomena were observed because nanosecond laser ablation of the material mainly relies on the rounding of the surface tension during the melting process, so the balling phenomenon is due to incomplete ablation [29].

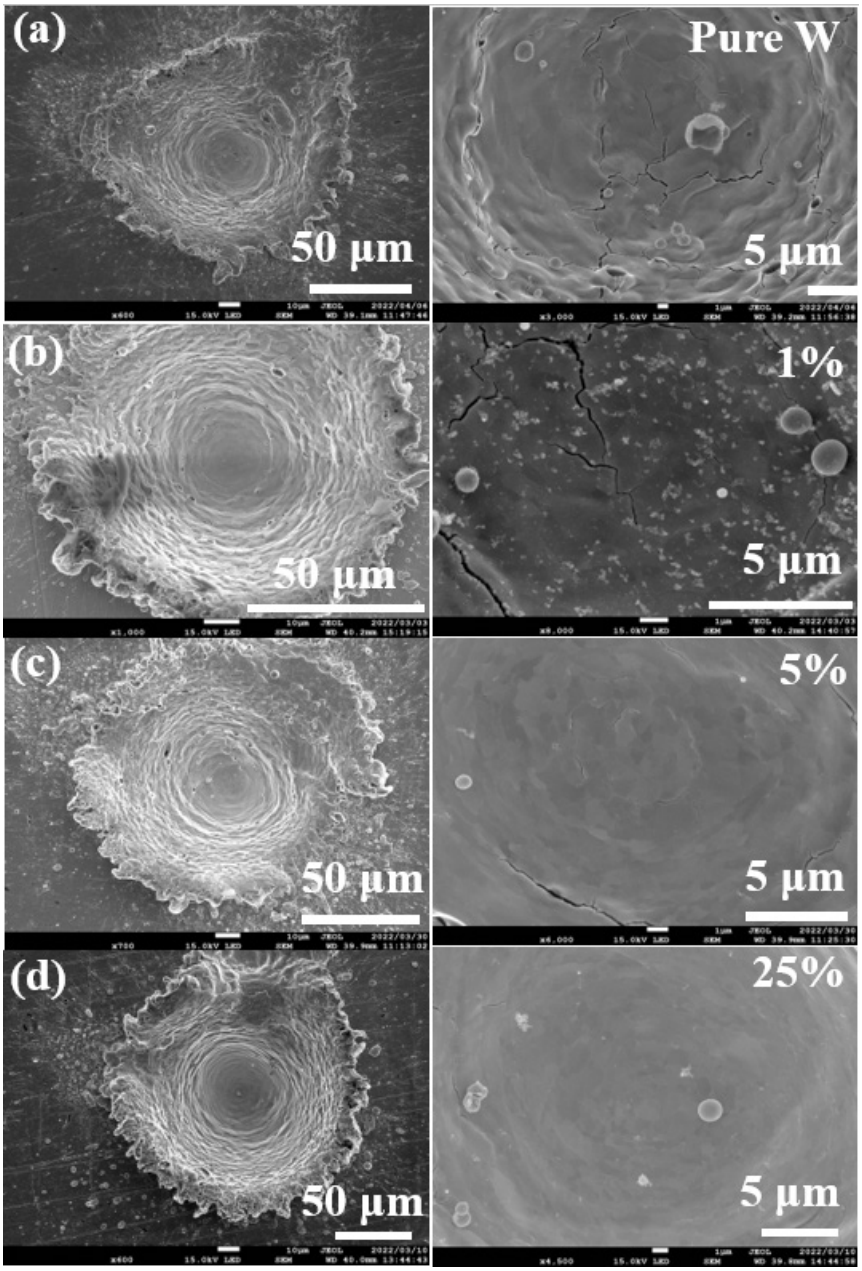

Fig. 2 SEM images of the development of holes generated by 100 pulses on various materials; (a) pure W, (b) W-1% Re, (c) W-5% Re, and (d) W-25% Re.

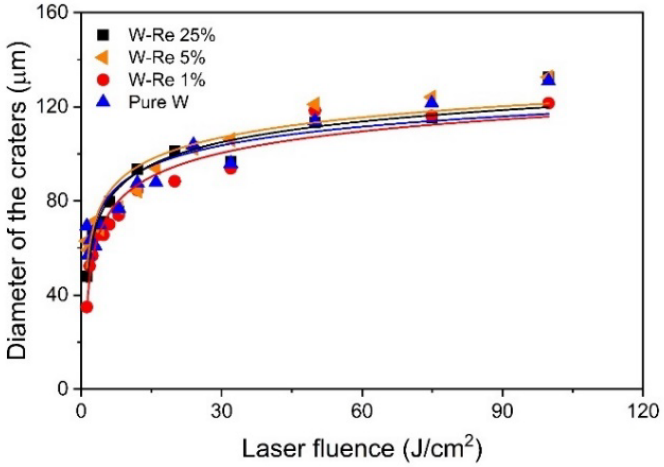

Fig. 3 Crater diameter in W-Re alloys and pure W as a function of laser fluence for 100 pulses.

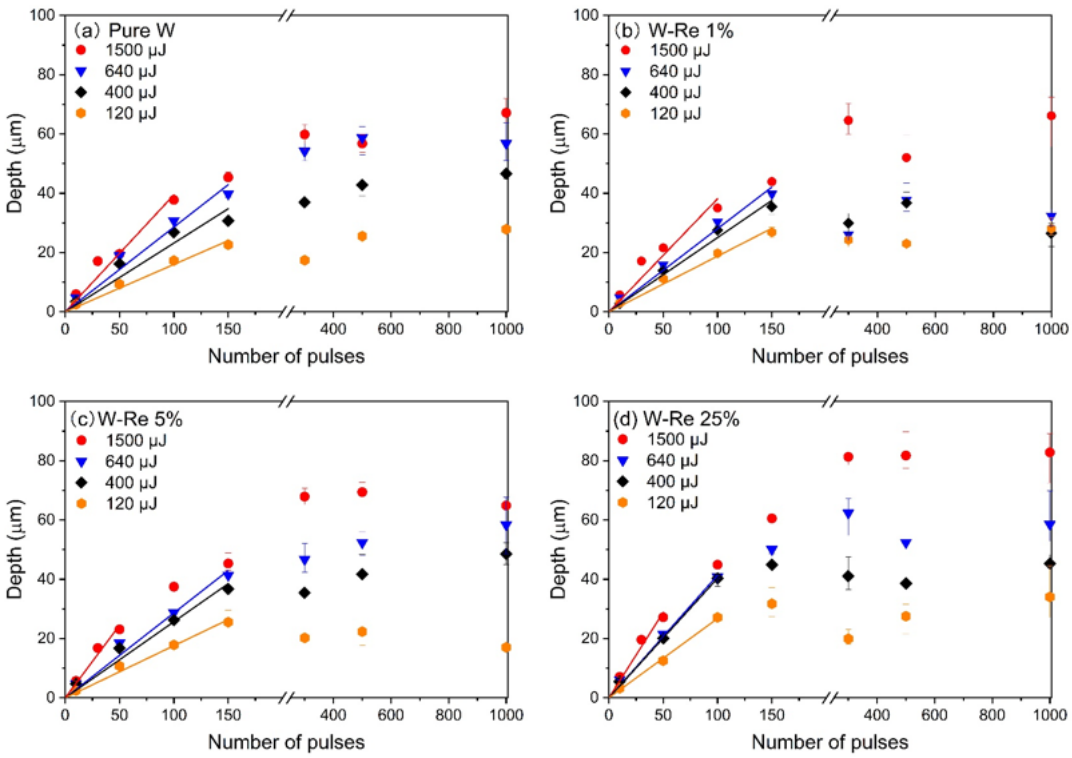

Fig. 4 Relationship between the hole depth and the number of pulses in pure W and W-Re alloys at various laser fluence.

The laser fluence dependence of the processing diameter is expressed as [30]:

$$\Gamma = a\sqrt{\ln(\frac{F}{F_{th}})}, \qquad (1)$$

where Γ is the diameter of the processed crater, a is the laser diameter at the irradiation position, F is the applied laser fluence, and F_{th} is the ablation threshold.

Figure 3 shows the dependence of the laser machined crater diameter on the applied laser fluence. The fitted curve has two distinct sections, which is due to the different ablation mechanisms. The first section is characterized by a relatively low ablation depth and high ablation rate with laser fluences from 1 J/cm^2 to 15 J/cm^2, and the diameter of the crater grows rapidly in this section. When the laser fluence exceeds 15 J/cm^2, the fitted curve shows a saturation trend because this section is characterized by a relatively high ablation depth and low ablation rate [31].

The dependence of the laser processing depth on the number of laser pulses for W-Re alloys with different doping concentrations is shown in Fig. 4. For all samples, the processing depth increases almost linearly with an increase in the number of pulses. When more than a certain pulse is applied to a W-Re alloy and pure tungsten, the slope of the ablation rate is significantly reduced. This occurs when the laser machined hole size is not significantly different from the laser spot size (diameter: 50 μm) because the laser energy is then distributed over a larger area, which results in a lower effective fluence [14,32].

The toughness of the W-Re alloys increases [25] and the hardness decreases as the Re doping concentration increases, which makes it easier to perform laser ablation. Therefore, the samples with the highest Re doping concentration had the deepest machining depths. At relatively low Re doping concentrations of 5% and 1%, no obvious difference in processing depth was evident for pure tungsten.

The dependence of the ablation rate on the laser fluence can be expressed as [30]:

$$R = \alpha^{-1}\ln(\frac{F}{F_{th}}), \qquad (2)$$

where R is the ablation rate, α^{-1} is the effective penetration depth of the laser fluence, and F and F_{th} are the laser fluence and ablation threshold, respectively. Figure 5 shows the ablation properties of pure W and W-Re alloys. Fitting of the ablation rates was performed with approximately ten different pulse energies. For all processed materials, the ablation rate increased almost linearly with the laser fluence in the range from 1 J/cm^2 to 100 J/cm^2 on the logarithmic scale. The ablation thresholds were 1.1 J/cm^2 for pure W, 0.9 J/cm^2 for W-1% Re, 0.9 J/cm^2 for W-5% Re, and 0.7 J/cm^2 for W-25% Re. The effective penetration depth for pure W was 86 nm, 85 nm for W-1% Re, 74 nm for W-5% Re, and 120 nm for W-25% Re.

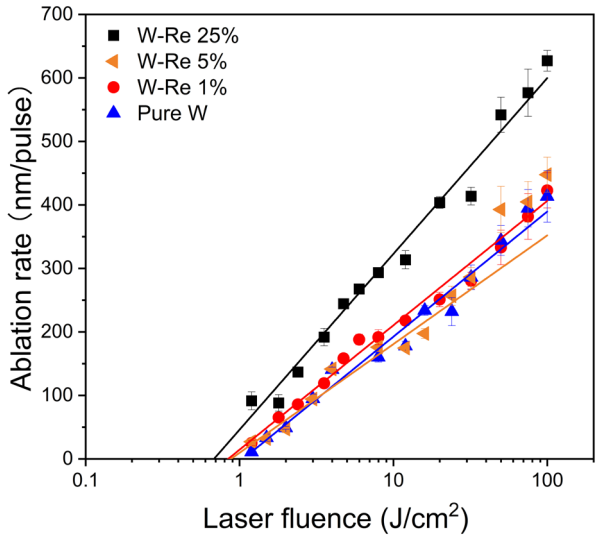

Fig. 5 Dependence of the ablation rate of pure W and W-Re alloys on the laser fluence given in a logarithmic scale.

A nanosecond laser system as the processing light source was employed in these experiments. A higher ablation threshold was obtained than that with a femtosecond laser system [14] due to the different physical mechanisms for the removal of material. Femtosecond processing uses mainly multiphoton nonlinear absorption and ionization in the microprocessing area to achieve microprocessing of any material without heat transfer because the time constant of electron-phonon coupling in metal is around several picoseconds. However, in the nanosecond regime, the laser energy couples with phonons, so that the lattice temperature increases, which results in melting and an evaporation process. Therefore, femtosecond processing is highly dependent on the work function that contributes to plasma formation. On the other hand, nanosecond processing is significantly affected by thermal properties such as the melting point, boiling point, and thermal conductivity, as the temperature increases. Therefore, the ablation threshold for the femtosecond processing of pure W is lower than that for nanosecond processing. In nanosecond processing, the W-Re alloy has a lower ablation threshold, despite having a higher work function. In addition, among all the W-Re alloys, the 25% Re-doped W-Re alloy with the lowest melting point (3100 °C) had the lowest ablation threshold, and the greatest ablation depth and ablation rate. Another possible explanation is the enhanced plastic mobility of the W-Re alloys, increased dislocation mobility, and increased ductility and toughness due to Re doping. Therefore, the W-Re alloy is more easily ablated by laser processing. In addition, the similar ablation threshold and ablation depth of the 1% and 5% doped W-Re alloys are due to the relatively low Re doping into W. However, from the results of SEM observations (see Fig. 2), the inhibitory effect of Re doping on laser processing cracks is still obvious; higher Re-doped W-Re alloys have better inhibitory effects on cracks.

4. Conclusion

The ablation properties of pure W were characterized using a 532 nm nanosecond Nd:YAG laser. The first laser processing of W-Re alloys was also demonstrated and the ablation properties of W-Re alloys were characterized. The W-Re alloy with a Re-doping concentration of 25% had the lowest ablation threshold of ca. 0.7 J/cm^2, the deepest effective penetration depth of ca. 120 nm, the largest ablation rate of ca. 650 nm/pulse, and a better crack inhibition ability. We consider that W-Re alloys with better mechanical properties are promising candidates for next-generation nuclear fusion reactor materials, and as such, research on the laser processing of W-Re alloys will become a hot topic in the near future.

Acknowledgments and Appendixes

This research was supported by a grant (No.20K05374) from the Japan Society for the Promotion of Science (JSPS), New Energy and Industrial Technology Development Organization (NEDO), Frontier Photonic Sciences Project of National Institutes of Natural Sciences (No.01212209), Research Foundation for Opto-Science and Technology, and the National Institute for Fusion Science (KIEH002, UFEX106, MISS201).

References

[1] W. E. Forsythe and A. G. Worthing: Astrophys. J., 61, (1925) 146.

[2] Shuhei Nogami, Akira Hasegawa, Makoto Fukuda, Michael Rieth, Jens Reiser, and Gerald Pintsuk: J. Nucl. Mater., 543, (2021) 152506.

[3] M. Rieth, S.L. Dudarev, S.M. Gonzalez de Vicente, J. Aktaa, T. Ahlgren, S. Antusch, D.E.J. Armstrong, M. Balden, N. Baluc, M.-F. Barthe, W.W. Basuki, M. Battabyal, C.S. Becquart, D. Blagoeva, H. Boldyryeva, J. Brinkmann, M. Celino, L. Ciupinski, J.B. Correia, A. De Backer, C. Domain, E. Gaganidze, C. García-Rosales, J. Gibson, M.R. Gilbert, S. Giusepponi, B. Gludovatz, H. Greuner, K. Heinola, T. Höschen, A. Hoffmann, N. Holstein, F. Koch, W. Krauss, H. Li, S. Lindig, J. Linke, Ch. Linsmeier, P. López-Ruiz, H. Maier, J. Matejicek, T.P. Mishra, M. Muhammed, A. Muñoz, M. Muzyk, K. Nordlund, D. Nguyen-Manh, J. Opschoor, N. Ordás, T. Palacios, G. Pintsuk, R. Pippan, J. Reiser, J. Riesch, S.G. Roberts, L. Romaner, M. Rosin´ ski, M. Sanchez, W. Schulmeyer, H. Traxler, A. Ureña, J.G. van der Laan, L. Veleva, S. Wahlberg, M. Walter, T. Weber, T. Weitkamp, S. Wurster, M.A. Yar, J.H. You, and A. Zivelonghi: J. Nucl. Mater. 432, (2013) 482.

[4] R. Villaria, V. Barabash, F. Escourbiacb, L. Ferrand, T. Hirai, V. Komarov, M. Loughlin, M. Merola, F. Moro, L. Petrizzi, S. Podda, E. Polunovsky, and G. Brolatti: Fusion Eng. Des., 88, (2013) 2006.

[5] T. Hirai, F. Escourbiac, S. Carpentier-Chouchana, A. Fedosov, L. Ferrand, T. Jokinen, V. Komarov, A. Kukushkin, M. Merola, R. Mitteau, R.A. Pitts, W. Shu, M. Sugihara, B. Riccardi, S. Suzuki, and R. Villari: Fusion Eng. Des. 88, (2013) 1798.

[6] P. Lickschat, D. Metzner, and S. Weißmantel: Int.J. Adv. Manuf. Technol., 109, (2020) 1167.

[7] K. E. Hazzan, M. Pacella, and T. L. See: Micromachines-basel, 12, (2021) 895.
[8] A. Alhuzaim, S. Imbrogno, and M. M. Attallah: Mater. Des. 211, (2021) 110123.
[9] J.-M. Drezet, M.S.F. Lima, J.-D. Wagnière, M. Rappaz, and W. Kurz: Proc. of the IIW Conference, (2008) 87.
[10] S. Paul, R. Singh, and W. Yan: "Lasers Based Manufacturing" ed. by S. N. Joshi and U. S. Dixit (Springer, India,2015) p.139.
[11] Z. Wu, H. Bao, Y. Xing, and L. Liu: Int. J. Adv. Manuf. Technol., 114, (2021) 1241.
[12] M. Stafe, I. Vladoiu, C. Negutu, and I. M. Popescu: Rom. Rep. Phys., 60, (2008) 789.
[13] P. Simon and J. Ihlemann: Appl. Phys. 63, (1996) 505.
[14] J. Byskov-Nielsen, J.-M. Savolainen, M. S. Christensen, and P. Balling: Appl Phys A, 101, (2010) 97.
[15] N. Lasemi, U. Pacher, L.V. Zhigilei, O.Bomati-Miguel, R. Lahoz, and W. Kautek: Appl. Surf. Sci., 433, (2018) 772.
[16] G. Dumitru, B. Lu¨scher, M. Krack, S. Bruneau, J. Hermann, and Y. Gerbig: Int. J. Refract. Met. H., 23, (2005) 278.
[17] F. Fazliana, S.N. Aqida, and I. Ismail: Opt. Laser Technol., 121, (2020) 105789.
[18] M.S. Komlenok, N.R. Arutyunyan, C. Freitag, E.V. Zavedeev, A.D. Barinov, M.L. Shupegin, and S.M. Pimenov: Opt. Laser Technol., 135, (2021) 106683.
[19] K. Tsuchida, T. Miyazawa, A. Hasegawa, S. Nogami, and M. Fukuda: Nucl. Mater. Eng., 15, (2018) 158.
[20] M. Fukuda, T. Tanno, S. Nogami, and A. Hasegawa: Mater. Trans., 53, (2012) 2145.
[21] T. Leonhardt: JOM., 61, (2009) 68.
[22] A. Kepceoğlu, Y. Gündoğdu, A. Sarilmaz, M. Ersöz, F. Özel, and H. Ş. Kiliç: Turk. J. Chem., 45, (2021) 485.
[23] Chester T. Sims, Charles M. Craighead, and Robert I. Jaffee: JOM., 7, (1955) 168.
[24] A. Hasegawa, M. Fukuda, T. Tanno, and S. Nogami: Mater. Trans., 54, (2013) 466.
[25] P.Rama Rao: "Phase diagram of binary tungsten alloys" ed. by S.V. Nagender Naidu and P.Rama Rao, (Indian Institute of Metals, India, 1991).
[26] https://www.americanelements.com/tungsten-rhenium-alloy-12299-18-2
[27] Katherine C. Phillips, Hemi H. Gandhi, Eric Mazur, and S. K. Sundaram: Adv. Opt. Photonics, 7, (2015) 684.
[28] S. Watanabe, S. Nogami, J. Reiser, M. Rieth, S. Sickinger, S. Baumgärtner, T. Miyazawa, and Akira Hasegawa: Fusion Eng. Des., 148, (2019) 111323.
[29] X. Zhou, X. Liu a, D. Zhang, Z. Shen, and W. Liu: J. Mater. Process Tech., 222, (2015) 33.
[30] H. Masaki: J. Plasma Fusion Res. 94, (2018) 244.
[31] L. Qi, K. Nishii, M. Yasui, H. Aoki, and Y. Namba: Opt. Laser Eng., 48, (2010) 1000.
[32] C.S. Nielsen and P. Balling: J. Appl. Phys., 99, (2006) 093101.

(Received: June 21, 2022, Accepted: November 13, 2022)